IOP Publishing Journal of Physics: Condensed Matter
J. Phys.: Condens. Matter **30** (2018) 385701 (7pp) https://doi.org/10.1088/1361-648X/aada53

Pressure-induced enhancement in the superconductivity of $ZrTe_3$

HPSTAR 618-2018

Kemin Gu[1,2,3], Resta A Susilo[1,3], Feng Ke[1], Wen Deng[1], Yanju Wang[1], Lingkong Zhang[1], Hong Xiao[1] and Bin Chen[1]

[1] Center for High Pressure Science and Technology Advanced Research, Pudong, Shanghai 201203, People's Republic of China
[2] Graduate School, China Academy of Engineering Physics, Beijing 100088, People's Republic of China

E-mail: chenbin@hpstar.ac.cn

Received 16 May 2018, revised 21 July 2018
Accepted for publication 15 August 2018
Published 29 August 2018

Abstract

We report the superconductivity enhancement of $ZrTe_3$ on compression up to 33 GPa. The superconducting transition occurs above 4.1 GPa and the superconducting temperature (T_C) increases with pressure in further compression, reaching a maximum of 7.1 K at ~28 GPa. An anomalous change of superconducting temperature is seen in the compression above 21 GPa. No structural phase transition is observed in the whole compression up to 36 GPa, but a subtle change in structural parameter is seen between 17–19 GPa, which seems relevant to the anomalous increase in the superconducting temperature. First-principle calculations reveal that the density of states at the Fermi level increases with pressure, which explains the enhancement of T_C in $ZrTe_3$ under compression.

Keywords: superconductivity, high pressure, transition metal trichalcogenides

(Some figures may appear in colour only in the online journal)

1. Introduction

2D transition metal (M) trichalcogenides MX_3 (X = S, Se, Te) have become an interesting platform to study the interplay between charge density wave (CDW) and superconductivity (SC). CDW are known to present in NbS_3 [1] and TaS_3 [2] whereas $NbSe_3$ exhibits SC on cooling below 2.1 K [3]. The competing interaction between the CDW state and SC in MX_3 is known to be sensitive with the application of pressure, such as in the case of $NbSe_3$, where SC can be induced as the CDW state is suppressed by pressure [4]. Among MX_3 system, $ZrTe_3$ has emerged as an intriguing compound to investigate, as it provides a rare example where the CDW and SC can coexist without any chemical or structural modifications. $ZrTe_3$ exhibits metallic behavior at room temperature, and shows both the presence of CDW at T_{CDW} ~ 63 K and SC below $T_C = 2$ K [5–7]. The SC was attributed to be a filamentary in nature with no diamagnetic signal in a small applied magnetic field [7].

Several attempts have been made to tune the interplay between CDW and SC in $ZrTe_3$, for example by intercalation, substitution and disorder. Upon intercalation of Cu, Ni and Ag, the filamentary SC of undoped $ZrTe_3$ turns into a bulk SC, with T_C of 3.8 K, 3.1 K and 5.1 K, respectively [8–10]. The CDW coexists with SC in Cu_xZrTe_3 [8] while it is suppressed as the bulk SC appears in Ni_xZrTe_3 [9]. Substitution of Te with Se in $ZrTe_{3-x}Se_x$ revealed the emergence of SC as the CDW is suppressed upon Se doping [11]. Disorder also can tune $ZrTe_3$ into bulk SC which is accompanied by the suppression of CDW [12].

Pressure is known to be a powerful way to tune the interaction between CDW and SC in $ZrTe_3$. Initial pressure study show the enhancement of T_{CDW} reaching a maximum of ~105 K at 1.1 GPa, while at the same time the filamentary SC disappears [13]. A dome-like behavior in T_{CDW} is observed at higher pressures up to 5 GPa, above which the CDW suddenly disappear and a bulk SC emerges, providing evidence for a pressure-induced re-entrant SC [14]. Raman spectroscopy studies suggest the occurrence of a structural phase transition accompanying the pressure-induced CDW to SC transition [15]. However, no such indication of a structural

[3] These authors contributed equally to this work.

 © 2018 IOP Publishing Ltd Printed in the UK

phase transition was observed from x-ray diffraction (XRD) measurements up to 6 GPa [16]. Despite these high pressure investigations, previous studies were limited to pressures below 12 GPa. This aspect renders our understanding on what happens to the superconducting state of $ZrTe_3$ at higher pressures, in particular whether the SC state will be suppressed or enhanced in the higher pressure regime remains unknown.

Here, we report the results of our study to investigate the evolution of SC in $ZrTe_3$ up to ~33.3 GPa. We found that the superconducting temperature is increased on compression, and no sign of suppression of SC is observed up to the highest pressure of measurement of ~33 GPa. On compression around 21 GPa, we found an enhancement of SC reaching a maximum T_C ~ 7 K at ~28 GPa which remains relatively constant up to ~33 GPa.

2. Methods

The $ZrTe_3$ single crystals were purchased from the 2D Semiconductors Company. The sample was crystallized to a bulk form with 1 mm in thickness and 5 × 5 mm in size. Energy dispersive spectrum was employed to detect the composition of the sample. The obtained atomic ratio is Zr:Te = 1:2.98, which is close to the expected stoichiometric ratio. In order to determine one surface normal to the sample, single crystal XRD was measured with Cu Kα radiation using a PANalytical X-Pert Pro diffractometer, following a method by Jesche *et al* [17].

The resistivity data of single crystal sample at high pressure was measured in a diamond anvil cell made of Be–Cu non-magnetic alloy. The size of the diamond culet was 300 μm in diameter. Be–Cu gasket was initially pre-indented to a thickness of 35 μm, then a hole of 280 μm was drilled using laser drilling system. A mixture of epoxy and cubic boron nitride (cBN) powder was pressed into the hole to form an insulating layer between the electrodes and the Be–Cu gasket. A hole of 120 μm in diameter was re-drilled in the cBN + epoxy gasket as a sample chamber. $ZrTe_3$ single crystal was cut into a square of 50 μm in width with 10 μm in thickness. We used the van der Pauw four probe method to measure electrical resistance using platinum (Pt) foil as electrodes. In order to ensure a quasi-hydrostatic condition, we used silicon oil as a pressure-transmitting medium. Several ruby balls were loaded into the sample chamber as pressure calibrants [18].

High-pressure synchrotron powder XRD ($\lambda = 0.6199$ Å) was performed at room temperature at Beamline 12.2.2 in the Advanced Light Source at Lawrence Berkeley National Laboratory. The patterns were collected using a MAR 3450 type detector. Neon was used as a pressure transmitting medium and ruby balls as pressure calibrants for synchrotron XRD experiments. The DIOPTAS [19] program was used for image integrations and the Le Bail method was employed to fit the XRD data using the Fullprof program [20, 21]. First-principles calculations were performed using a Material Studio CASTEP module. The generalized gradient approximation was utilized for the exchange correlation potential [22].

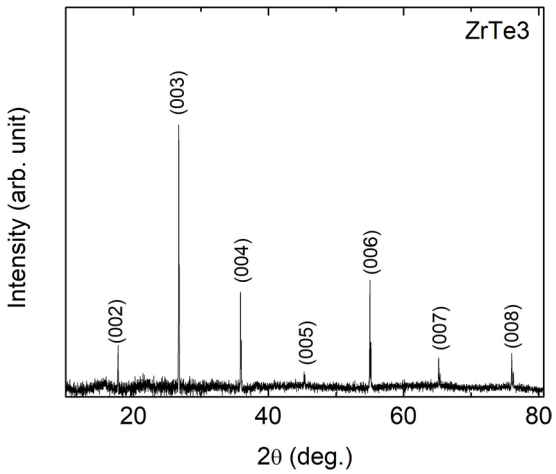

Figure 1. XRD pattern of single crystal $ZrTe_3$ collected at ambient condition.

3. Results and discussions

The XRD pattern of single crystal $ZrTe_3$ is shown in figure 1. All the diffraction peaks match the $(0\,0\,l)$ peaks belonging to the monoclinic $ZrTe_3$ phase (PDF Card No. 802224) which indicates that the surface of the crystal is perpendicular to the c-axis with the plate-shaped surface parallel to the ab-plane. In figure 2(a), we show resistivity $R(T)$ data obtained at various pressure points between 4 GPa and 33 GPa with the electric current applied on the crystal ab-plane. The resistivity data at 4.1 GPa shows a typical metallic behavior with a linear decrease in resistivity as the temperature is lowered. We observed an appearance of a broad peak at ~40 K which can be related to T_{CDW} as reported previously [13, 14]. Upon increasing pressure, this CDW state disappears and we observed a drop in resistance at 8.2 GPa, signaling a pressure-induced re-entrant SC [14]. The onset of SC still exists to the highest pressure of ~33 GPa.

Low temperature resistivity (2 K–10 K) of $ZrTe_3$ collected at various pressures between 8 GPa to 33 GPa is shown in figure 2(b). The onset of SC at 8.2 GPa is 4.3 K which then increases to ~6 K at 15 GPa, above which it is relatively constant as the pressure is increased to 23 GPa. A slight difference in T_C compared with previous report [14] might be due to the difference in hydrostatic condition. On compression above 23 GPa, we observe a sudden increase of T_C from 6 K to 7 K at 27.7 GPa. Further compression until 33 GPa does not change T_C. In figure 8(a), we show the evolution of the onset temperature of SC (T_C, onset) as a function of pressure. Anomalous enhancement of T_C is observed on compression above ~21 GPa. It also can be seen that the maximum of T_C occurs at around 27.7 GPa.

The appearance of SC in $ZrTe_3$ at high pressures (above 15 GPa) is further confirmed by our resistivity measurements under different applied magnetic fields, as shown in figure 3(a). Zero-resistance at 20.7 GPa, observed at zero magnetic field, is gradually lifted with increasing magnetic field, resulting in a decrease of T_C. Superconducting state is almost fully suppressed by an application of magnetic field of 3.15 T (figure 3(a)). The upper critical field, H_{c2}, determined

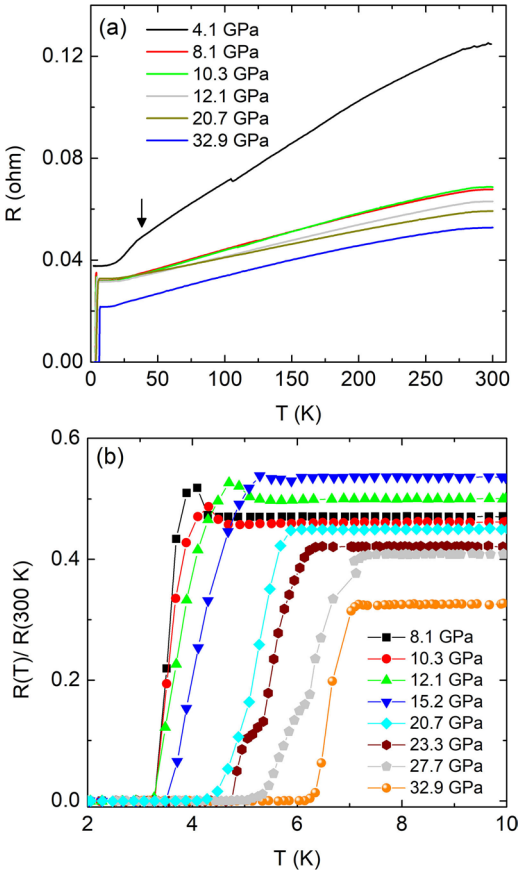

Figure 2. (a) The resistance of $ZrTe_3$ between 2 K and 300 K measured at various pressures. The arrow indicates a possible charge-density-wave transition reported previously [14]. (b) Low temperature part of the normalized resistivity of $ZrTe_3$ under high pressure up to 33 GPa.

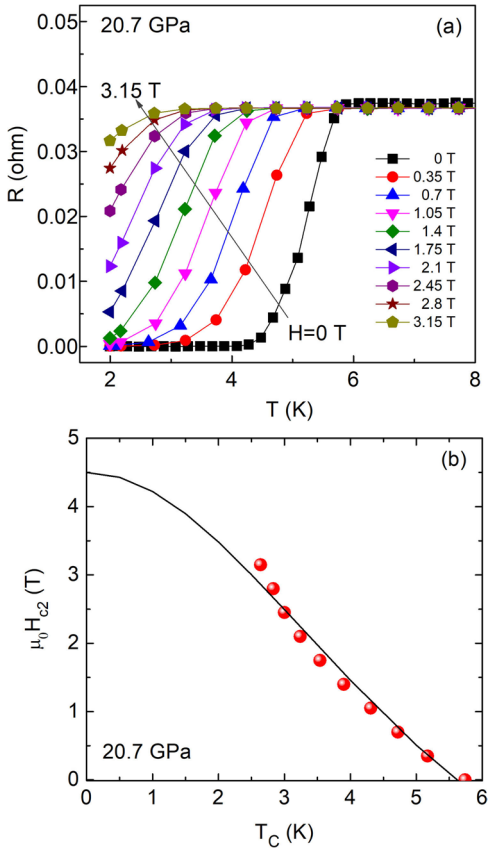

Figure 3. (a) Temperature dependence of resistance of $ZrTe_3$ under different applied magnetic fields up to 3.15 T at 20.7 GPa. (b) Temperature dependence of upper critical fields of $ZrTe_3$. In this case, T_C is determined as the onset of superconducting transition. The solid line represents a fit to the data using the Ginzburg–Landau (GL) formula.

using the onset of the resistivity drop (T_C, onset) are plotted in figure 3(b). Using the conventional one band Werthamer–Helfand–Hohenberg (WHH) model, the upper critical field at $T = 0$ K is given by $\mu_0 H_{c2}(0) = -0.693\ T_C \times (\mathrm{d}\mu_0 H_{c2}/\mathrm{d}T)$ [23], where $(\mathrm{d}\mu_0 H_{c2}/\mathrm{d}T)$ is the intial slope at T_C. The value of $(\mathrm{d}\mu_0 H_{c2}/\mathrm{d}T)$ is determined to be $-0.81(2)$ T K^{-1}, which leads to the value of $\mu_0 H_{c2}(0) = 3.1\,(2)$ T. The H_{c2} versus T curve was then fitted with the empirical expression based on the Ginzburg–Landau (GL) theory (e.g. [24]) which takes the form

$$\mu_0 H_{c2}(T) = \mu_0 H_{c2}(0)\,\frac{1-\left(\frac{T}{T_c}\right)^2}{1+\left(\frac{T}{T_c}\right)^2}. \qquad (1)$$

It can be seen that the data in figure 3(b) can be fitted relatively well using equation (1). The fitted value of $\mu_0 H_{c2}(0)$ is 4.5(1) T at 20.7 GPa. It is interesting to mention that a positive curvature close T_C is observed in a compressed $ZrTe_3$, which suggests a possible multiband superconducting pairing, similar to those observed in 2H–$NbSe_2$ and 2H–NbS_2 [25, 26]. From the value of $\mu_0 H_{c2}(0)$, the coherence length $\xi(0)$ can be estimated with Ginzburg–Landau formula $\mu_0 H_{c2}(0) = \Phi_0/(2\pi\xi(0)^2)$ where $\Phi_0 = 2.07 \times 10^{-15}$ Wb is the flux quantum. The estimated GL coherence length at 20.7 GPa is 8.6 nm, which is comparable to those observed in the intercalated $ZrTe_3$ single crystals [8–10]. We note that our derived value of $\mu_0 H_{c2}(0)$ is well below the Pauli limiting field for a singlet pairing of $\mu_0 H_P(0) = 1.84 T_c$ [27], i.e. 10.3 T for $T_C = 5.6$ K.

In order to investigate the possible correlation between structural properties and SC, we performed synchrotron XRD experiments under pressure up to 36.3 GPa. The collected XRD patterns are shown in figure 4(a). Due to the strong preferred orientation of the compressed $ZrTe_3$ sample, all XRD patterns were refined using the Le Bail method. It can be seen that the ambient crystal structure of $ZrTe_3$ (monoclinic $P2_1/m$ space group) is stable under compression until ~23 GPa. On compression above 23 GPa, we observed the splitting of two peaks at $2\theta \sim 13°$ and 17°, respectively, hinting a possible phase transition (indicated by asterisks in figure 4(a)). However, the splitting of these two peaks resembles what is observed in the patterns taken at the lower pressure region ($P < 15$ GPa), which suggests that $ZrTe_3$ still retains its monoclinic structure even above 25 GPa. We have attempted to index these new diffraction patterns in order to search for a possible crystal structure using indexing softwares, however the attempts always led to the same monoclinic structure. Recent high pressure studies on the isomorphic TiS_3 revealed an isostructural phase transition without any change in the

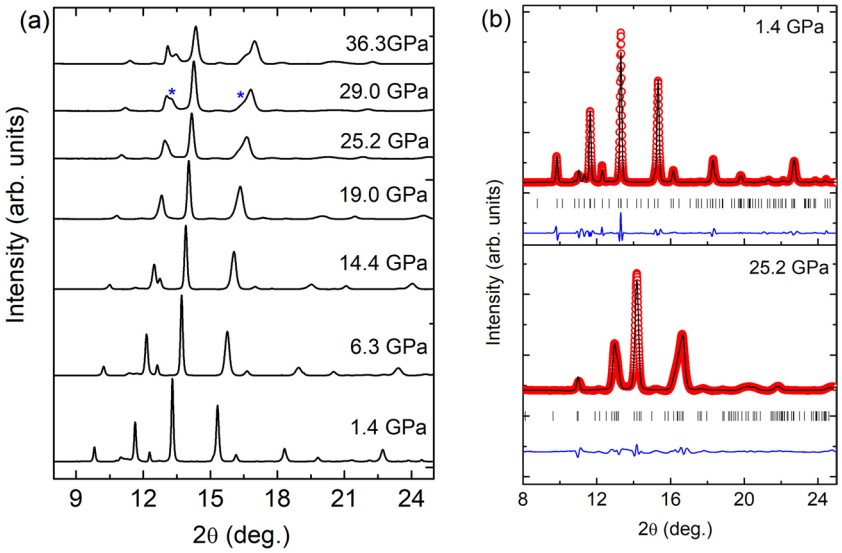

Figure 4. (a) Synchrotron XRD patterns of $ZrTe_3$ collected at various pressures up to 36.3 GPa. (b) Representative refinement of the patterns collected at 1.4 GPa and 25.2 GPa.

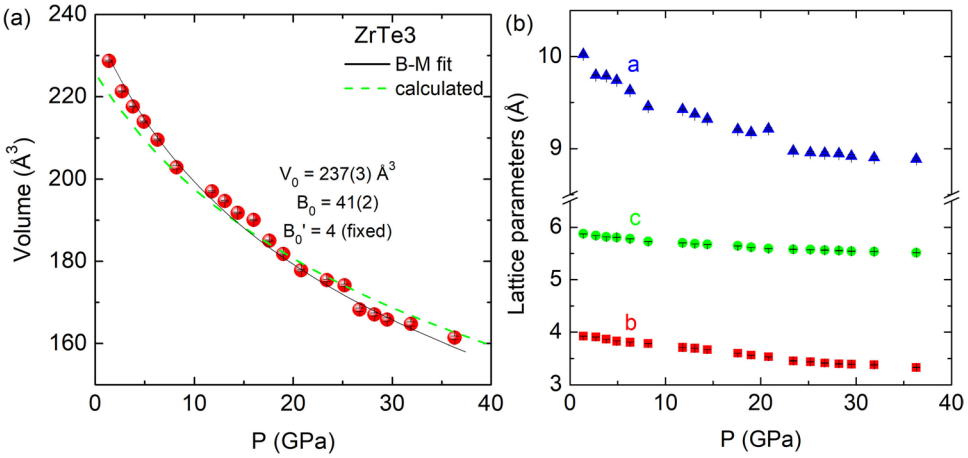

Figure 5. (a) Unit cell volume of $ZrTe_3$ as a function of pressure. Solid lines are fits to the data based on third-order Birch–Murnaghan formula as in equation (2). Dashed line represents the calculated pressure-dependence of the unit cell volume based on geometry optimizations. (b) Pressure dependence of the experimental lattice parameters (a)–(c).

space group under compression [28] which suggests that similar isostructural transition could also occurs in $ZrTe_3$. Hence, we fitted the XRD patterns above 23 GPa using the same monoclinic phase, and found that the patterns can be fitted with an identical space group. Selected fitting results using the Le Bail method to the patterns at 1.4 and 25.2 GPa are shown in figure 4(b).

The derived unit cell volume of $ZrTe_3$ as a function of pressure ($V(P)$) is shown in figure 5(a). The unit cell volume was fitted using the third-order Birch–Murnaghan (B–M) equation of state which takes the form [29, 30]

$$P = \frac{3}{2}B_0\left[\left(\frac{V_0}{V}\right)^{\frac{7}{3}} - \left(\frac{V_0}{V}\right)^{\frac{5}{3}}\right]\left\{1 - \left(3 - \frac{3}{4}B_0'\left[\left(\frac{V_0}{V}\right)^{\frac{2}{3}} - 1\right]\right)\right\} \quad (2)$$

where V_0, B_0, and B_0' are the unit cell volume, bulk modulus, and first-order derivative of the bulk modulus at zero pressure, respectively. The fitting to the whole $V(P)$ data using B–M equation as in equation (2) yields $V_0 = 237(3)$ Å^3 and $B_0 = 41(2)$ GPa, whereas the value of B_0' are fixed to 4. The experimentally derived lattice parameters are plotted in figure 5(b). All lattice parameters gradually decrease with the application of pressure. The lattice c parameter decreases faster than other lattice parameters due to the weak van der Walls bonding along the crystal c-direction.

From figure 5(a), it can be seen that the fitting of the $V(P)$ data using a single third-order B–M equation does not lead to a satisfactory result. The fitting results can be improved by considering two separate B–M equations, each of which is used to fit the data above and below 23 GPa (where the peak splitting occurs). However, the fitting parameters seem to be inconclusive given the lack of data points above 23 GPa. In order to better track the changes in the $V(P)$ curve derived from the XRD data, we transformed the $V(P)$ data into an Eulerian stress–strain $F(f)$ diagram based on the following formula [31–33]

$$F = P[3f(1+2f)^{5/2}]^{-1}, \quad (3)$$

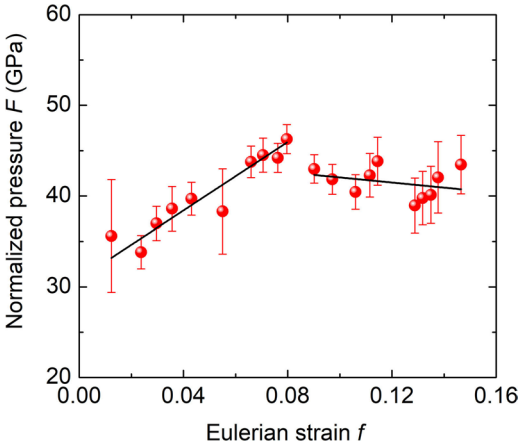

Figure 6. Normalized pressure (F) versus Eulerian strain (f) of $ZrTe_3$ derived with the volume at ambient pressure (V_0) derived from the fitting of the $V(P)$ data using third-order B–M equation. Solid lines are fits to the data using equation (5).

$$f = \frac{1}{2}\left[\left(\frac{V}{V0}\right)^{-2/3} - 1\right], \tag{4}$$

where f is the Eulerian strain, F is the corresponding normalized pressure, and V_0 is the volume at ambient pressure as determined from the B–M fitting. The values of B_0 and B_0' can be determined from the relationship between f and F described as

$$F = B_0 + {}^1\!/_2\ [3B_0\,(B_0' - 4)\,f]\,. \tag{5}$$

From equation (5), it can be seen that $F(f)$ curve will be linear and the values of B_0 and B_0' can be determined from the intercept as $F \to 0$ and the slope, respectively. In the case of structural tranformation, even a subtle one, the $F(f)$ plot will show a change in slope [33].

The $F(f)$ plot of $ZrTe_3$ is presented in figure 6. Different than the $V(P)$ data, the $F(f)$ plot shows a clear change in slope above Eulerian strain value of 0.08, which corresponds to $P \sim$ 18 GPa. This change in slope indicates a change in mechanical properties which might be related to a subtle structural transformation. Linear fitting to the two set of data ($f < 0.08$ and $f > 0.08$) yields $B_0 = 30.9(9)$ GPa and $B_0' = 8.1(3)$ (for the phase below 18 GPa), and $B_0 = 44(3)$ GPa and $B_0' = 3.6(4)$ (for the phase above 18 GPa).

Comparing this result with the pressure-dependence of T_C (shown in figure 8(a)), it can be seen that there is a correlation between the anomalous enhancement of T_C at high pressures and the change in the structural properties. T_C of $ZrTe_3$ begins to enhance anomalously on compression above ~21 GPa (indicated by arrow in figure 8(a)), and the mechanical properties, as observed from the $F(f)$ plot, reveal a change in slope above ~18 GPa. This indicates that the anomalous enhancement of T_C in $ZrTe_3$ on compression above ~21 GPa has a structural origin. We note that the difference in the transition pressure between these two experimental results are mostly due to the different hydrostatic conditions of the pressure mediums used (Neon for XRD experiments and silicon oil for high pressure electrical transport measurements).

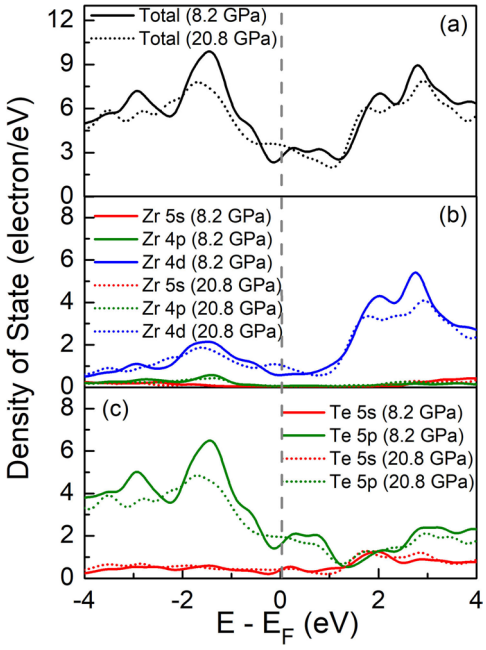

Figure 7. (a) Calculated total density of states of $ZrTe_3$ at 8.2 GPa and 20.8 GPa, and the partial density of states for Zr (b) and Te (c) atoms at 8.2 GPa and 20.8 GPa. Vertical line indicates the Fermi energy.

In order to better understand the evolution of SC, we performed first-principles calculations to study the effects of pressure to the electronic structure of $ZrTe_3$ under pressure. Here, we will only focus on the effects of pressure to the density of states at the Fermi level. Geometry optimizations of the lattice parameters and all the atomic coordinates are performed for each hydrostatic pressure point. The calculated unit cell volume at 1.4 GPa (224 Å^3) is only 2.1% smaller than the experimental value (228 Å^3). The theoretical bulk modulus is 52.1 GPa (shown as a dashed line in figure 5(a)), which is somewhat smaller than the experimentally derived bulk modulus using the B–M equation, i.e. 41 GPa. Such deviations are known to exist in generalized gradient approximation calculations.

The total and partial density of states of $ZrTe_3$ calculated at 8 and 21 GPa are shown in figure 7. It can be seen that the total density of states at the Fermi level ($N(E_F)$) is dominated by the Te 5p state mixed with the Zr 4d state, consistent with the previous report [34]. Increasing pressure from 8 GPa to 21 GPa, increases hybridization and bandwidth as seen by the reduction of the density of states above and below E_F. Interestingly, $N(E_F)$ increases gradually with increasing pressure due to the increases of Zr 4d and Te 5p states at E_F. The change of the Zr 4d states at E_F is more pronounced than that of the Te 5d states, which suggests that the SC may be hosted by the Zr 4d states inside the $ZrTe_3$ prisms.

The calculated total density of states at the Fermi level ($N(E_F)$) as a function of pressure is shown in Figure 8(b). It can be seen that $N(E_F)$ of $ZrTe_3$ shows a strong pressure dependence. It begins to increase at around 5 GPa, where the bulk SC initially appears under pressure [14]. $N(E_F)$ keeps increasing under compression, reaching a maximum at about

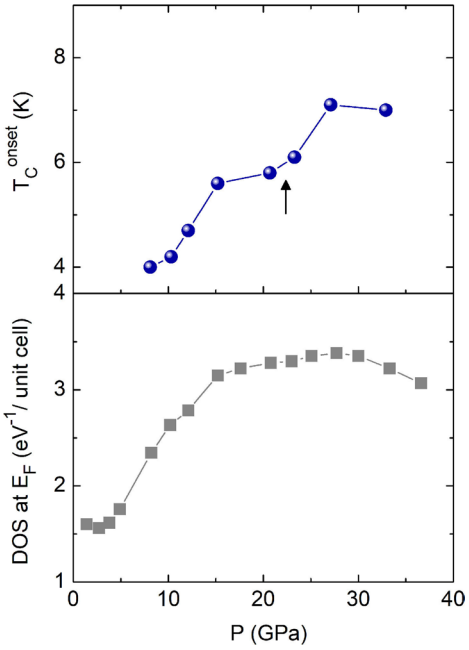

Figure 8. (a) Onset temperature of the superconducting transition in $ZrTe_3$ as a function of pressure. Arrow indicates the pressure above which T_C enhances anomalously. (b) The evolution of the calculated density of states at the Fermi level at high pressure.

27 GPa, above which it gradually decreases as the pressure is increased.

Based on the McMillan theory [35], the increase in the superconducting temperature is mostly contributed by the increase in the density of states at the Fermi level and the decrease in the characteristic phonon frequency. Previous Raman spectroscopy study up to 4 GPa revealed that the characteristic phonon frequency tend to increase under pressure [15], however no Raman spectroscopy studies on $ZrTe_3$ at higher pressures have been reported to date. Under the assumption that the phonon frequency of $ZrTe_3$ increases at higher pressure, the results shown in figures 8(a) and (b) suggest that the enhancement of T_C in $ZrTe_3$ under compression can be explained by the increase in $N(E_F)$. Therefore, it appears that the increase in $N(E_F)$ is the dominant contribution to the increase of T_C in $ZrTe_3$ under pressure. It would be of interest to investigate the Raman spectroscopy experiments on $ZrTe_3$ at higher pressure to investigate the charateristic phonon frequency. It would also be beneficial to calculate the phonon density of states of $ZrTe_3$ under pressure.

4. Conclusion

We have studied the evolution of SC in $ZrTe_3$ at high pressures up to 33 GPa. With increasing pressure, T_C raises from ~4 K reaching a maximum value of 7.1 K at ~28 GPa, above which T_C remains constant up to 33 GPa. We found no sign of obvious structural phase transition up to 36 GPa, however a change in mechanical properties was observed on compression above ~18 GPa, which seems to correlate with the anomalous increase in T_C above 21 GPa. Density of states at the Fermi level increases gradually with pressure which explain the enhancement of SC in $ZrTe_3$ at high pressures.

Acknowledgments

We thank Dr Zhiqiang Chen (HPSTAR) for the helpful discussions. The authors acknowledge the use of beamline 12.2.2 at the Advanced Light Source, Lawrence Berkeley National Laboratory. The authors would also like to thank the reviewers for their comments and suggestions which improved the quality of the paper.

ORCID iDs

Kemin Gu https://orcid.org/0000-0001-5434-9468
Hong Xiao https://orcid.org/0000-0001-8859-9967

References

[1] Wang Z *et al* 1989 *Phys. Rev.* B **40** 11589
[2] Ido M, Tsutsumi K, Sambongi T and Mori N 1979 *Solid State Commun.* **29** 399–402
[3] Yamamoto M 1978 *J. Phys. Soc. Japan* **45** 431–8
[4] Monceau P, Peyrard J, Richard J and Molinié P 1977 *Phys. Rev. Lett.* **39** 161
[5] Takahasi S and Sambongi T 1983 *J. Phys.* **44** 1733
[6] Takahasi S and Sambongi T 1984 *Solid State Commun.* **49** 1031
[7] Nakajima H, Nomura K and Sambongi T 1986 *Physica* B **143** 240
[8] Zhu X, Lei H and Petrovic C 2011 *Phys. Rev. Lett.* **106** 246404
[9] Lei H, Zhu X and Petrovic C 2011 *Europhys. Lett.* **95** 17011
[10] Yadav C S and Paulose P L 2012 *J. Phys.: Condens. Matter* **24** 235702
[11] Zhu X *et al* 2016 *Sci. Rep.* **6** 26974
[12] Zhu X, Lv B, Wei F, Xue Y, Lorenz B, Deng L, Sun Y and Chu C-W 2013 *Phys. Rev.* B **87** 024508
[13] Yamaya K, Yoneda M, Yasuzuka S, Okajima Y and Tanda S 2002 *J. Phys.: Condens. Matter* **14** 10767–70
[14] Yomo R, Yamaya K, Abliz M, Hedo M and Uwatoko Y 2005 *Phys. Rev.* B **71** 132508
[15] Gleason S L *et al* 2015 *Phys. Rev.* B **91** 155124
[16] Hoesch M, Garbarino G, Battaglia C, Aebi P and Berger H 2016 *Phys. Rev.* B **93** 125102
[17] Jesche A, Fix M, Kreyssig A, Meier W R and Canfield P C 2016 *Phil. Mag.* **96** 2115–24
[18] Mao H K, Xu J and Bell P M 1986 *J. Geophys. Res.* **91** 4673
[19] Prescher C and Prakapenka V B 2015 *High Pressure Res.* **35** 223
[20] Roisnel T and Rodríguez-Carvajal J 2001 *Mater. Sci. Forum* **118** 378
[21] Rodríguez-Carvajal J 1993 *Physica* B **192** 55
[22] Perdew J P, Burke K and Ernzerhof M 1996 *Phys. Rev. Lett.* **77** 3865
[23] Werthamer N R, Helfand E and Hohenberg P C 1966 *Phys. Rev.* **147** 295–302
[24] Fang L, Wang Y, Zou P Y, Tang L, Xu Z, Chen H, Dong C, Shan L and Wen H H 2005 *Phys. Rev.* B **72** 014534
[25] Suderow H, Tissen V G, Brison J P, Martínez J L and Vieira S 2005 *Phys. Rev. Lett.* **95** 117006
[26] Tissen V G, Osorio M R, Brison J P, Nemes N M, García-Hernández M, Cario L, Rodière P, Vieira S and Suderow H 2013 *Phys. Rev.* B **87** 134502
[27] Clogston A M 1962 *Phys. Rev. Lett.* **9** 266
[28] An C *et al* 2017 *Phys. Rev.* B **96** 134110
[29] Murnaghan F D 1937 *Am. J. Math.* **59** 235

[30] Birch F 1947 *Phys. Rev.* **71** 809
[31] Soignard E, Shebanova O and McMillan P F 2007 *Phys. Rev.* B **75** 014104
[32] Salamat A, Briggs R, Bouvier P, Petitgirard S, Dewaele A, Cutler M E, Corà F, Daisenberger D, Garbarino G and McMillan P F 2013 *Phys. Rev.* B **88** 104104
[33] Woodhead K, Pascarelli S, Hector A L, Briggs R, Aldermanc N and McMillan P F 2014 *Dalton Trans.* **43** 9647
[34] Felser C, Finckh E W, Kleinke H, Rocker F and Tremel W 1998 *J. Mater. Chem.* **8** 1787
[35] McMillan W L 1968 *Phys. Rev.* **167** 331